Turing instability mediated by voltage and calcium diffusion in paced cardiac cells

Yohannes Shiferaw[†‡] and Alain Karma[§]

[†]UCLA Cardiovascular Research Laboratory, Department of Medicine (Cardiology), David Geffen School of Medicine, University of California, Los Angeles, CA 90095; and [§]Department of Physics and Center for Interdisciplinary Research on Complex Systems, Northeastern University, Boston, MA 02115

In cardiac cells, the coupling between the voltage across the cell membrane (V_m) and the release of calcium (Ca) from intracellular stores is a crucial ingredient of heart function. Under abnormal conditions and/or rapid pacing, both the action potential duration and the peak Ca concentration in the cell can exhibit well known period-doubling oscillations referred to as "alternans," which have been linked to sudden cardiac death. Fast diffusion of V_m keeps action potential duration alternans spatially synchronized over the ≈150-μm-length scale of a cell, but slow diffusion of Ca ions allows Ca alternans within a cell to become spatially asynchronous, as observed in some experiments. This finding raises the question: When are Ca alternans spatially in-phase or out-of-phase on subcellular length scales? This question is investigated by using a spatially distributed model of Ca cycling coupled to V_m. Our main finding is the existence of a Turing-type symmetry breaking instability mediated by V_m and Ca diffusion that causes Ca alternans to become spontaneously out-of-phase at opposite ends of a cardiac cell. Pattern formation is governed by the interplay of short-range activation of Ca alternans, because of a dynamical instability of Ca cycling, and long-range inhibition of Ca alternans by V_m alternans through Ca-sensitive membrane ionic currents. These results provide a striking example of a Turing instability in a biological context where the morphogens can be clearly identified, as well as a potential link between dynamical instability on subcellular scales and life-threatening cardiac disorders.

arrhythmias | cardiac dynamics | nonlinear dynamics | pattern formation

When a cardiac cell is stimulated by a change in the membrane, V_m, calcium (Ca) is released from intracellular stores and signals cell contraction (1, 2). This release of Ca occurs within several thousand submicrometer-scale junctions distributed throughout the volume of the cell. Within these junctions localized clusters of Ca-sensitive ion channels called Ryanodine receptors, which gate the flow of Ca across intracellular stores, open in response to Ca entry via L-type Ca channels in the surface cell membrane (1). Signaling within these junctions occurs through a Ca-induced–Ca-release process (2, 3), which endows the system with rich spatiotemporal properties typical of excitable media.

Rapid pacing rates, or abnormal physiological conditions, are known to produce complex dynamics of both V_m and Ca at the cell and tissue level. The most common nontrivial dynamics is the phenomenon of alternans, where the action potential duration (APD) and the Ca transient alternate from one beat to the next (4, 5). Alternans is clinically important because it has been shown to correlate with the onset of life-threatening arrhythmias and sudden cardiac death (6, 7). Historically, alternans has been attributed to a period-doubling instability that depends on the electrical restitution properties of cardiac cells (4, 8, 9), which itself is governed by the kinetics of membrane ion currents. More recent studies, however, have demonstrated that alternans also can result from an instability of intracellular Ca cycling (5, 10–12).

Recently, Kockskamper and Blatter (13) used two-dimensional (2D) line-scan confocal microscopy of cat atrial cells to image the spatial distribution of Ca release when the cell was paced during alternans. They observed that the release of Ca could be spatially out-of-phase, where one half of the cell alternated with opposite phase with the other half. Out-of-phase subcellular Ca alternans also has been observed by Diaz *et al.* (14) in rat ventricular cells. These experimental results demonstrate that Ca release within cells can form complex spatiotemporal patterns. However, what governs the formation and dynamics of these patterns remains unknown.

To address this question, we explore the spatiotemporal dynamics of Ca and V_m alternans using numerical simulations of a physiologically based ionic model. A distinguishing feature of this model, in comparison with previous models (10, 15, 16), is that it captures the spatially distributed nature of the Ca cycling system, along with a description of the membrane ion currents that couple to this system. Hence, this model can be used to investigate pattern formation of Ca signaling on subcellular scales. The simulations reveal that spatially distant regions of Ca alternans can either synchronize or spontaneously desynchronize depending on the bidirectional coupling between the intracellular Ca and V_m. This bidirectional coupling is mediated by Ca-sensitive membrane ionic currents that gate V_m. Because Ca mediates the contraction of the cardiac cell, these asynchronous subcellular patterns will influence contraction on the tissue scale and thus may potentially affect the function of the heart.

To shed light on this pattern formation process, we reduce the multivariable ionic model to coupled reaction–diffusion equations that govern the spatiotemporal evolution of the amplitudes of Ca and V_m alternans. These amplitude equations describe the spatiotemporal dynamics of Ca and APD alternans at the subcellular scale. An analysis of these equations reveals that the spatial desynchronization of Ca alternans results from a symmetry-breaking Turing-like instability (17–19) mediated by V_m and Ca diffusion. The amplitudes of alternans are shown to play the role of diffusing morphogens, with Ca corresponding to the short-range activator and V_m to the long-range inhibitor. The crucial requirement for a Turing instability, in which the inhibitor diffuses significantly faster than the activator, is ensured by the fact that V_m diffuses across the cell membrane ≈10^4 times faster than intracellular Ca in the myoplasm.

Physiologically Detailed Model

Cell Architecture. The architecture of a cardiac ventricular cell is shown schematically in Fig. 1*A*. The cell membrane forms an array of deep invaginations into the cell (t-tubules), distributed along planes (z-lines) transverse to the long axis of the cell (20). The t-tubules distribute dyadic junctions, where Ca signaling takes place, uniformly over the cell volume. The volume in between z-lines is referred to as the sarcomere and contains the sarcoplasmic reticulum (SR). The SR is a diffuse tubular network that sequesters a high concentration of Ca. A typical ventricular myocyte has a length of 150 μm and has ≈75–100 sarcomeres.

We take advantage of the observed structural periodicity in the

---

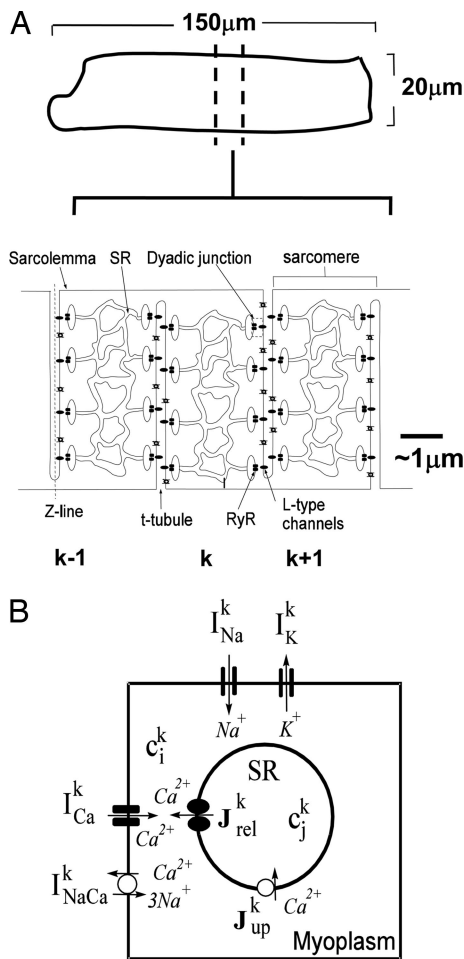**Fig. 1.** Illustration of cardiac cell architecture and ionic model. (*A*) Schematic representation of the structure of the cardiac cell. The cell is divided into subcellular units, which correspond to sarcomeres. (*B*) Illustration of Ca cycling machinery along with ion currents that regulate V_m within a sarcomere.

longitudinal direction to treat each sarcomere as an equivalent subcellular unit. This method lets us represent the cell as a 1D chain of identical subunits, where each subunit is assumed to have an identical distribution of dyadic junctions, and to enclose a roughly equivalent volume of the SR network. We assume further that Ca diffusion is sufficiently fast on the scale of one sarcomere, so that the concentration of Ca can be accurately described by the local spatial average. Note that atrial cells lack t-tubules, and consequently Ca release propagates as a wave from the cell membrane toward the central axis of the cell. We expect, however, the present model to also be applicable to these cells as long as this propagation time is shorter than the pacing period, in which case the cell can still be divided longitudinally into equivalent subunits.

V_m Dynamics. The effective diffusion coefficient of V_m ($D_V \approx 2.5 \times 10^{-4}$ cm^2/ms) (2) is large. Therefore, V_m equilibrates rapidly over the length scale of a cell on a time scale of ≈ 0.5 ms that is comparable with the rise time of the action potential (1 ms) but much smaller than the APD. Hence, we can assume that each sarcomere senses the same V_m, which is dictated by the ionic currents averaged over the whole cell. The membrane ionic currents, which govern the dynamics of V_m across the membrane surrounding a single sarcomere (here the *k*th subunit), are shown schematically in Fig. 1*B*. Here, I_{Na}^k is the fast inward Na$^+$ current, I_K^k is the total outward K current, and I_{Ca}^k and I_{NaCa}^k are the Ca-dependent L-type and NaCa exchange currents, respectively.

The ionic currents are formulated by using the canine ventricular cell model of Fox *et al.* (15), which is based on Luo–Rudy currents (16). The spatially uniform V_m across the cell membrane satisfies the standard equation of charge-conservation

$$\frac{dV_m}{dt} = -\frac{1}{C_m} \sum_{k=1}^{N} (I_{Na}^k + I_{Ca}^k + I_K^k + I_{NaCa}^k + I_{stim}), \quad [1]$$

where C_m is the cell membrane capacitance, and N is the number of sarcomere units. Because the V_m-dependent Na and K currents do not couple to the intracellular Ca transient, they are spatially uniform along the cell. Therefore, the sums over I_{Na}^k and I_K^k in Eq. **1** can be replaced by the whole cell current. In contrast, Ca-dependent currents are local and vary between sarcomeres. I_{stim} is a stimulus current applied to the whole cell simultaneously, consistent with the fact that V_m is assumed to be spatially uniform. A detailed formulation of these ionic currents is in *Supporting Text*, which is published as supporting information on the PNAS web site.

Ca Cycling Dynamics. The Ca cycling dynamics within each sarcomere is described by using the model of Shiferaw *et al.* (10). The essential elements of the local Ca cycling machinery are shown in Fig. 1*B*. Ca entry into the sarcomere occurs via L-type Ca channels (I_{Ca}^k), which triggers a Ca-induced–Ca release flux (J_{rel}^k) from Ryanodine receptor channels bound to the SR membrane. The amount of Ca released into the sarcomere depends sensitively, in a nonlinear fashion, on the concentration in the SR (the SR-load c_j^k). Once the intracellular Ca concentration (c_i^k) rises, powerful uptake (J_{up}^k) pumps on the SR membrane are activated and pump Ca back into the SR. The Ca that enters the cell via I_{Ca}^k is extruded out of the cell via the electrogenic NaCa exchange current (I_{NaCa}^k), so that at steady state, Ca entry balances Ca extrusion. The Ca systems in neighboring sarcomeres are coupled by allowing diffusion between the Ca in myoplasm (c_i^k) and SR (c_j^k). Ca diffusion ($D_{Ca} = 150$–300 μm^2/s) (2) is several orders of magnitude slower than V_m diffusion driven by voltage gradients along the cell. Full details of the Ca cycling model are described in *Supporting Text*.

Bidirectional Coupling. The coupling of V_m to the local Ca transient within a sarcomere is determined by the experimentally established phenomenon of graded SR Ca release (1, 21), where the amount of SR Ca released increases in proportion to the local Ca entry (I_{Ca}^k). The availability of L-type Ca channels at a given beat depends on the previous diastolic interval, which is the time spent at full repolarization before the next action potential upstroke. Now, a larger diastolic interval gives more time for recovery of L-type Ca channels at the resting membrane potential. Thus, in our sarcomere model, graded release requires that the peak of the local Ca transient increases in response to an increase of diastolic interval in the previous beat, as illustrated in Fig. 2*A*. This coupling will be referred to hereafter as "positive $V_m \rightarrow$ Ca coupling." In principle, it is also possible to have the opposite effect at slow pacing rate, also illustrated in Fig. 2*A* ("negative $V_m \rightarrow$ Ca coupling"). However, we did not investigate this case in the present study.

The local Ca released into a sarcomere also couples to the global APD by its effect on the local membrane ionic currents. As discussed in ref. 22, there are two cases that need to be considered. The first, referred to as "positive Ca $\rightarrow V_m$ coupling," illustrated in Fig. 2*B*, corresponds to the case when a large local Ca release tends to prolong the APD. The second, referred to as "negative Ca $\rightarrow V_m$ coupling" (Fig. 2*B*), corresponds to the case when a large local Ca release shortens the APD. The sign of the coupling is dictated by the relative contributions of the local L-type Ca current (I_{Ca}^k) and the NaCa exchange current (I_{NaCa}^k) to the APD. A larger Ca release tends to inactivate the local I_{Ca}^k more rapidly through Ca-induced inactivation, which tends to shorten the APD. However, a large local Ca release also increases I_{NaCa}^k, which tends to prolong APD.
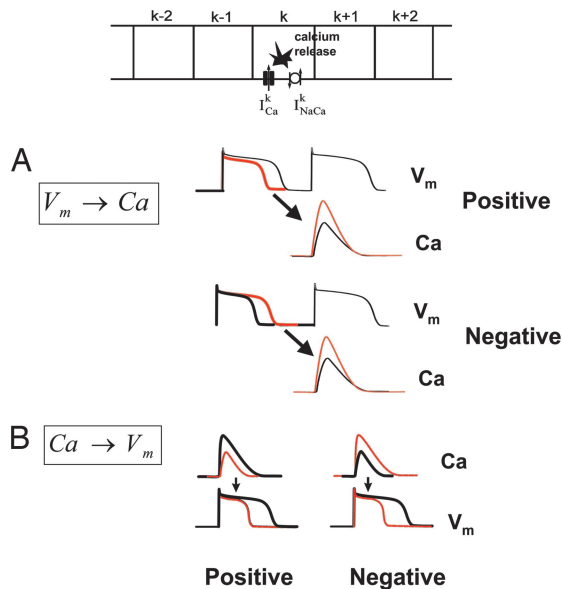
Fig. 2. Illustration of bidirectional coupling between Ca and V_m. (*A*) Coupling between the APD and the Ca transient on the next beat. (*B*) Coupling between the Ca transient and the APD on the same beat.

For the ionic model used here, the sign of the coupling was controlled by adjusting the degree of Ca-induced inactivation of the I_{Ca}^k, as described in *Supporting Text*.

Alternans. Steady-state alternans of the Ca transient within a given sarcomere can be induced in the model by increasing the steepness, at high SR loads, of the function relating SR Ca release to SR Ca load, as described theoretically (10, 11) and experimentally (12). In experiments under physiologically normal conditions (5), and in the present ionic model, this bifurcation to alternans occurs at rapid pacing rates ($T < T_c$) when the cell is overloaded with Ca. For low pacing rates $T > T_c$, the steady-state Ca transient is periodic from beat-to-beat.

Alternans also can be induced by a purely V_m-dependent mechanism, independently of Ca cycling. This mechanism depends on the kinetics of membrane ion currents, which regulate V_m, and are typically described using the restitution relationship between APD and diastolic interval (4, 8). However, in our study we found that alternans due to the latter mechanism always yielded spatially synchronized Ca alternans. The reason for this result is that when the spatially uniform APD alternates, it simply drives local Ca alternans in phase over the extent of the cell by means of the graded coupling described in the previous section. Hence, in this study, we have focused exclusively on alternans due to unstable Ca cycling, which we found leads to nontrivial spatial patterns.

The bidirectional coupling between the APD and the local Ca release determines the relative phase of APD and Ca transient alternans at the subcellular level (23–25). For alternans due to unstable Ca cycling, positive Ca $\rightarrow V_m$ coupling produces steady-state electromechanically concordant alternans, where a large–small–large local Ca transient corresponds to long–short–long APD, whereas negative Ca $\rightarrow V_m$ leads to steady-state electromechanically discordant alternans, where a small–large–small peak Ca transient corresponds to a long–short–long APD. Both of these modes of alternans have been observed experimentally under various physiological conditions (23–25).

Numerical Results

We have simulated a set of $N = 75$ coupled sarcomeres with a spacing of $\Delta = 2$ μm between Z-planes and a cell length $L = N\Delta =$
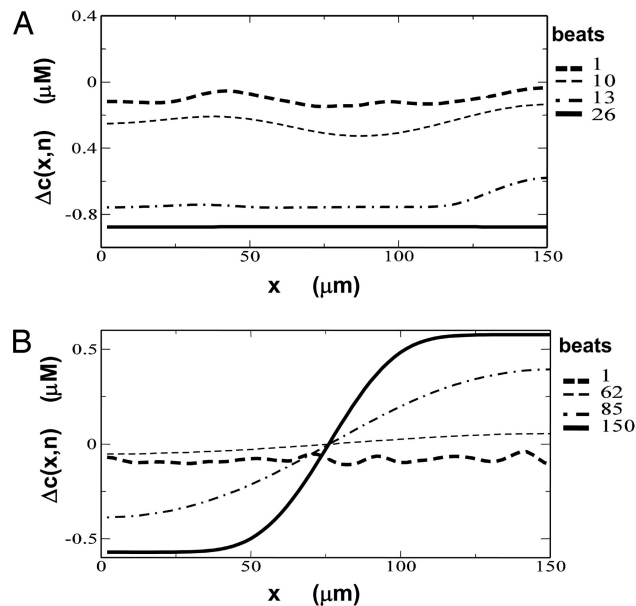

Fig. 3. Spatiotemporal dynamics of subcellular Ca alternans in a cell with 75 sarcomeres for two different strengths of Ca-induced inactivation of the L-type Ca current. (*A*) Weak Ca-induced inactivation (positive Ca $\rightarrow V_m$ coupling) leads to spatial synchronization of alternans. The thick black line corresponds to the steady-state Ca alternans amplitude. The pacing rate is 0.35 s, with $T_c = 0.37$ s. (*B*) Strong Ca-induced inactivation (negative Ca $\rightarrow V_m$ coupling) leads to spontaneous symmetry breaking resulting in desynchronization of two halves of the cell. The pacing rate is 0.35 s, with $T_c = 0.344$ s. Detailed parameters of the ionic model are given in Tables 1–7, which are published as supporting information on the PNAS web site.

150 μm. To characterize the spatiotemporal evolution of Ca alternans, we define the local amplitude of Ca alternans as $\Delta c(x, n) = (-1)^n(c_{n+1}^k - c_n^k)$, where c_n^k is the peak Ca transient in sarcomere k at the nth paced beat, and where $x = k\Delta$ denotes the position along the cell. The factor $(-1)^n$ is included so that the phase of alternans does not change sign at every beat.

The parameters of the isolated sarcomere model are chosen such that, at a pacing rate $T < T_c$, alternans due to unstable Ca cycling develops and saturates at a steady-state value. The initial Ca concentration in the SR was chosen to be $\approx$10 μM less than its steady-state value, so that fully developed alternans emerged only after $\approx$100 paced beats, i.e., the SR had to load with Ca before it became dynamically unstable. Thus, for the first few beats, alternans amplitude of Ca and APD was always zero for all sarcomeres in the cell. To mimic realistic conditions, the initial conditions of Ca concentration in the myoplasm and the SR were taken from a Gaussian distribution with a standard deviation <1% of their average value.

Our main finding is that the final steady-state pattern of Ca alternans depends sensitively on the bidirectional coupling between Ca and V_m. When model parameters were chosen such that the Ca $\rightarrow V_m$ coupling was positive, steady-state Ca alternans were always in-phase over the extent of the cell. In Fig. 3*A*, we plot the amplitude of Ca alternans in a cell where the degree of Ca-induced inactivation is adjusted so that the Ca $\rightarrow V_m$ coupling was positive. The spatial distribution of the amplitude of Ca alternans at the nth beat, $\Delta c(x, n)$, started at a very small value across the cell and grew as the cell was paced at $T = 0.35$ s to a fully developed spatially synchronized pattern. To assess the nature of the coupling for these model parameters, we paced an isolated sarcomere at the same rate and found that alternans were indeed electromechanically concordant. In contrast, when the Ca $\rightarrow V_m$ coupling was negative,
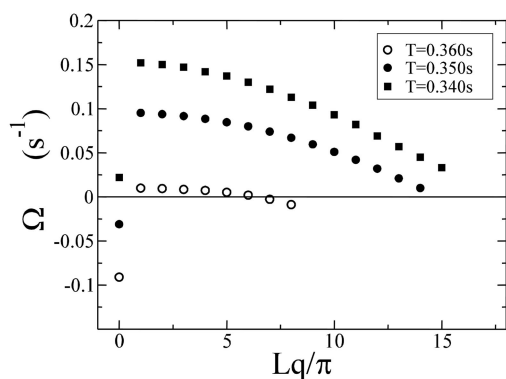
Fig. 4. Numerically computed linear stability spectrum showing the exponential amplification rate Ω of sinusoidal perturbations of the spatially uniform steady state with no alternans vs. the dimensionless wavenumber qL/π for different pacing periods $T = 0.34, 0.35,$ and 0.36 s. For all periods, the fastest-growing wavelength is twice the cell length ($q = \pi/L$). The model parameters are the same as those that yielded the asynchronous state in Fig. 3B.

spatially out-of-phase alternans developed from an initially small amplitude spatial distribution, as shown in Fig. 3B. In this case, the final steady-state pattern was such that the two halves of the cell alternated out of phase, and $\Delta c(x, n)$ changed sign across a node in the center of the cell. Remarkably, a qualitatively similar pattern was observed in the experiments of Kockskamper and Blatter (13). To assess the nature of the coupling for these parameters, we paced again an isolated sarcomere and found that Ca and APD alternans were electromechanically discordant.

To further analyze the pattern-formation mechanism that produces the asynchronous state for negative Ca $\rightarrow V_m$ coupling, we carried out numerically a linear stability analysis of the spatially homogeneous state with no alternans. We computed the amplification rate $\Omega(q)$ of small sinusoidal perturbations of wavelength $\lambda = 2\pi/q$ in a large system of $N = 400$ coupled sarcomeres. For each mode the amplification rate was obtained from the slope of a linear-log plot of the average magnitude of alternans, defined as $C(n) = \sqrt{1/N\Sigma_{k=1,N}\Delta c(k\Delta, n)^2}$, vs. time $t = nT$. The results of these simulations are shown in Fig. 4 where $\Omega(q)$ is plotted vs. the dimensionless wave number qL/π for three different pacing periods. For all periods, the mode with the largest wavelength, which is equal to twice the cell length, $qL/\pi = 1$, has the largest amplification rate. For $T = 0.35$ and 0.36 s, this mode is unstable, whereas the spatially homogeneous mode, $q = 0$, is stable. The latter follows from the fact that the onset of alternans for an isolated sarcomere is $T_c = 0.344$ s for the parameters used in these simulations. These results demonstrate that the asynchronous state results from a pattern forming linear instability.

Morphogenetic Roles of Ca and V_m Alternans

A basic understanding of this pattern forming instability can be gained by considering the similarity between the amplitudes of Ca and APD alternans and diffusing morphogens in a Turing-like instability. It is useful to discuss this analogy qualitatively to set the stage for amplitude equations in the next section, which provide the formal mathematical framework to make this analogy precise.

Activator. The fact that Ca diffuses much slower than V_m makes the amplitude of Ca alternans the natural candidate for short-range activator. This role can only be fulfilled, however, if the alternans within an isolated sarcomere are due to an intrinsic instability of Ca cycling rather than V_m dynamics. In this case, Ca transient alternans will grow locally as the cell is paced and induce APD alternans. In Fig. 5A, we show the beat-to-beat Ca transient and V_m during alternans for an isolated sarcomere that exhibits discordant electromechanical alternans. Next, consider a small fluctuation that
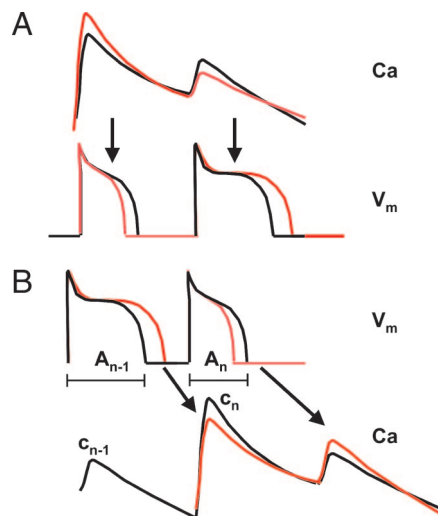
Fig. 5. Analogy to a Turing instability mechanism. (A) Ca alternans amplitude as short-range activator. The red line of the Ca trace corresponds to Ca alternans that have larger amplitude than that shown by the black line. The effect on the V_m trace is to increase the amplitude of APD alternans. (B) APD alternans amplitude as long-range inhibitor. An increase in APD alternans amplitude leads to a decrease in Ca alternans amplitude on the next beat.

leads to an increase in amplitude of Ca alternans, as indicated by the red trace. The subsequent feedback of Ca on V_m will tend to increase the amplitude of APD alternans, as long as the subsequent changes in APD do not feedback and cancel the effect of the small fluctuation on the next beat. This condition will be made more mathematically precise below but is essentially equivalent to saying that the feedback of Ca on itself should be stronger than the feedback of V_m on itself. If this condition is met, then the amplitude of Ca alternans can be viewed as the activator of APD alternans.

Inhibitor. The extremely fast diffusion of V_m in the cell membrane makes the amplitude of APD alternans the natural candidate for the long-range inhibitor. To study the effect of APD alternans on Ca transient alternans, consider a sarcomere in which alternans are electromechanically discordant, as illustrated by the black lines in Fig. 5B. The mathematical condition for this dynamical mode is that $\partial A_n/\partial c_n < 0$, where A_n and c_n denote the APD and peak Ca transient at beat n. This condition, which is equivalent to negative Ca $\rightarrow V_m$ coupling, ensures that an increase in peak Ca transient c_n tends to decrease the APD A_n, and thus a large Ca transient will correspond to a small APD and vice versa. A more rigorous mathematical derivation of this condition using a nonlinear map reduction is given in *Supporting Text* and Fig. 6, which is published as supporting information on the PNAS web site. Now consider a fluctuation that increases the amplitude of APD alternans, as illustrated by the red V_m trace in Fig. 5B. Such a fluctuation will cause the Ca transient peak in the next beat to be smaller if $\partial c_n/\partial A_{n-1} < 0$. This condition is equivalent to the requirement for positive $V_m \rightarrow$ Ca coupling as illustrated in Fig. 2A and is precisely the coupling dictated by the phenomenon of graded release incorporated in our detailed ionic model. The later decrease in the peak Ca transient is equivalent to a decrease in Ca alternans amplitude because the larger Ca peak (red line) is smaller than it would have been in the absence of the fluctuation (black line). Combining the above two conditions, we can conclude that for APD alternans to inhibit Ca transient alternans the condition $(\partial A_n/\partial c_n)(\partial c_n/\partial A_{n-1}) > 0$ must be satisfied. This condition also can be satisfied when alternans are electromechanically concordant if the sign of both partial derivatives are reversed, although this case was not explored here.

After identification of the amplitudes of Ca and APD alternans with diffusing morphogens, understanding the formation of the asynchronous state follows straightforwardly from the analogy with a classic Turing instability mechanism. Namely, a fluctuation that causes the amplitude of Ca alternans to increase in a small region of the cell generates APD alternans that in turn inhibit the growth of Ca alternans far from that localized fluctuation (long-range inhibition). Thus, Ca alternans will not synchronize spatially under these conditions and will develop nontrivial spatiotemporal patterns.

Amplitude Equations

A more quantitative analytical understanding of the Turing instability can be obtained by deriving equations that govern the spatiotemporal evolution of the amplitudes of Ca and APD alternans (26). The derivation, which is detailed in *Supporting Text*, exploits the fact that the local beat-to-beat dynamics in the detailed ionic model can be described by an iterative map, and that the alternans amplitudes are small and evolve slowly (over many beats) close to the alternans bifurcation.

The starting point of the derivation is the 2D iterative map $A_n = F_1(A_{n-1}, c_n)$, and $c_n = F_2(A_{n-1}, c_{n-1})$, which relates the APD and peak Ca transient at one beat to the next. Such a map was recently shown to describe well the beat-to-beat dynamics of V_m and Ca in a situation where the APD and Ca transient are assumed to be spatially uniform (22). Here, we allow these quantities to vary spatially and label each sarcomere by its position x along the cell. We couple the maps spatially using nonlocal spatial kernels that describe the cumulative effect of V_m and Ca diffusion in the interval of one beat. For V_m, this coupling amounts to simply taking A_n equal to the spatial average of $A_n = F_1(A_{n-1}, c_n(x))$ owing to the fact that V_m diffusion is essentially instantaneous. For Ca, we take $c_n(x)$ to be the weighted average of $F_2(A_{n-1}, c_{n-1}(x'))$ with a weight that decreases smoothly to zero with increasing $|x - x'|$ over a length scale $\xi \sim (D_{Ca} \times T)^{1/2}$, where D_{Ca} is the average diffusion constant of free Ca inside the cell, and T is the pacing period. Next, we make the substitutions $A_n = A^* + (-1)^n a(n)$ and $c_n(x) = c^* + (-1)^n c(x, n)$ in the spatially coupled maps, where A^* and c^* are the fixed point of the map, and $a(n)$ and $c(x, n)$ are the amplitudes of APD and Ca alternans, respectively. We use the fact that the amplitudes of alternans vary slowly from beat to beat close to the alternans bifurcation to treat the beat number n, or equivalently the time $t = nT$ as a continuous variable, which allows us to write $A_{n+2} - A_n \approx 2T(-1)^n \partial a/\partial t$, and similarly $c_{n+2} - c_n \approx 2T(-1)^n \partial c/\partial t$. In addition, we assume that the amplitude of Ca alternans varies along the cell on a scale larger than the spacing between sarcomeres, such that x can be treated as a continuous variable. With these simplifications, we get

$$\frac{\partial a}{\partial t} = \alpha a + \beta \bar{c}, \qquad [2]$$

$$\frac{\partial c}{\partial t} = \gamma a + \mu \bar{c} + \delta c + D \partial_x^2 c, \qquad [3]$$

where $\bar{c} = (1/L)\int_0^L c(x, t)dx$ denotes the spatial average of the Ca alternans amplitude over the whole cell. For clarity, we have omitted nonlinear terms that are not essential to characterize the linear regime of the instability. The coefficients of the amplitude equations, which are derived in detail in *Supporting Text*, can be expressed in terms of the matrix elements of the Jacobian matrix of the two-variable map defined by $J_{11} = \partial F_1/\partial A_n, J_{12} = \partial F_1/\partial c_n$, $J_{21} = \partial F_2/\partial A_n$, and $J_{22} = \partial F_2/\partial c_n$, evaluated at the fixed point of the map A^* and c^*. The effective diffusion coefficient of Ca alternans amplitude is given by $D = J_{22}^2\xi^2/2T$.

It is important to emphasize that the reaction–diffusion Eqs. **2** and **3** have a richer structure than the standard Turing model (17, 19) because of the fact that the diffusing morphogens measure the

amplitude of period-doubling oscillations of two signals (Ca and V_m), rather than the concentrations of two chemical species. Consequently, the local rate of generation of the activator depends both on its local value and on its spatial average over the cell, as reflected by the appearance of terms proportional to c and $\bar{c}$ in Eq. **3**, respectively. In contrast, there is no analog of the global coupling term $\bar{c}$ in the equation for the activator in the limit of the standard Turing model where the inhibitor diffuses quasi-instantaneously on the scale of the system. It is interesting to note that, beyond the Turing analogy, the breakdown of synchronization leading to the formation of phase domains also has been found to occur generically in oscillatory media in the presence of global coupling, as observed in certain surface catalytic reactions (27).

The conditions for a Turing instability can now be readily obtained from a stability analysis of the amplitude equations. Taking a and c proportional to $\exp(iqx + \Omega(q)t)$, the condition for a nontrivial solution of Eqs. **2** and **3** to exist yields an eigenvalue equation for $\Omega(q)$ that is quadratic in q. The most unstable branch is easily found to be $2\Omega(0) = \alpha + \mu + \delta + \sqrt{(\alpha - \mu - \delta)^2 + 4\gamma\beta}$, and $\Omega(q) = \delta - Dq^2$ for $q \neq 0$. The two conditions for a finite wavelength instability are, first, that the fastest amplification rate of modes with $q \neq 0$ be positive, or here $\lim_{q\to 0}\Omega(q) = \delta > 0$, and, second, that this amplification rate is larger than that of the spatially homogeneous $q = 0$ mode, or $\delta > \Omega(0)$. Note that the analytically predicted stability spectrum $\Omega(q)$ is precisely of the form that was calculated numerically using the physiologically detailed model in Fig. 4 when these two conditions are satisfied (see Fig. 7, which is published as supporting information on the PNAS web site).

Physical Interpretation. To interpret the above conditions for a finite wavelength instability, we express the inequality conditions in terms of the Jacobian of the beat-to-beat map. The first condition, $\delta > 0$, is equivalent to $J_{22} < -1$, which corresponds physically to the condition that alternans are due to an instability in Ca cycling. The second condition, $\delta > \Omega(0)$, is shown in *Supporting Text* to be equivalent to the two conditions $J_{22} < J_{11}$ and $J_{12}J_{21} < 0$. Because J_{11} and J_{22} give a measure of the degree of instability of the V_m and Ca cycling subsystems, the first condition is satisfied if the Ca subsystem is effectively more unstable than the V_m subsystem, which makes the condition for Ca to be the activator more precise, as described in the last section. The second condition, $J_{12}J_{21} < 0$, is in turn equivalent to the condition for V_m to be the inhibitor, $(\partial A_n/\partial c_n)(\partial c_n/\partial A_{n-1}) > 0$, derived in the last section by using qualitative arguments. To see this condition, note that $J_{21} = \partial c_n/\partial A_{n-1}$, and $J_{12} = (\partial c_n/\partial c_{n-1})(\partial A_n/\partial c_n)$ and that $\partial c_n/\partial c_{n-1} = J_{22}$ is negative for alternans to occur.

Analysis of the leading eigenvector of the Jacobian reveals that the relative phase of Ca and APD alternans is determined precisely by the conditions above for the finite wavelength instability. Note that condition $J_{12}J_{21} < 0$ can be satisfied in two ways: $J_{12} < 0$ and $J_{21} > 0$ or $J_{12} > 0$ and $J_{21} < 0$. If $J_{21} < 0$, the condition for a finite wavelength instability is identical to that for electromechanically discordant alternans. This result is precisely the case investigated here where APD alternans inhibit Ca alternans, consistent with the qualitative arguments of the last section. If $J_{21} > 0$, the instability condition requires that alternans are electromechanically concordant. The latter case was not investigated here.

Comparison with Ionic Model. The physical interpretation of the amplitude equations is consistent with our numerical simulation results. The simulations revealed that the asynchronous state developed after many beats only when we enhanced the effect of Ca-induced inactivation. For the same model parameters, an isolated sarcomere paced at the same rate exhibited electromechanically discordant alternans. This dynamical mode emerged when alternans are due to a steep relationship between SR Ca release and SR load and when the Ca → V_m coupling is negative, as illustrated in Fig. 2B. Because, furthermore, the V_m → Ca coupling is positive

Shiferaw and Karma

in the ionic model by virtue of the graded release relationship between Ca release from the SR and the L-type Ca current, which triggers this release, the asynchronous state developed when $(V_m \rightarrow Ca) \times (Ca \rightarrow V_m) < 0$, which is equivalent to the condition $J_{12}J_{21} < 0$ for a Turing instability obtained from the amplitude equations.

Discussion

The main finding of this work is that heterogeneity of Ca cycling on the subcellular scale can arise spontaneously from a Turing-type instability mediated by Ca and V_m diffusion. In the present context, symmetry breaking is produced by local self-enhancement of Ca alternans and long-range inhibition of these alternans by APD alternans. Amplitudes of Ca and APD alternans are predicted to play a directly analogous role to activator and inhibitor species in the context of reaction–diffusion models in which Turing patterns have been studied (18). The crucial requirement that the inhibitor diffuses faster than the activator is fulfilled here because V_m diffusion is several orders of magnitude faster than Ca diffusion.

The conditions for this instability can be summarized as follows. (*i*) Alternans at the subcellular level must be due to an instability of Ca cycling. (*ii*) Bidirectional coupling derived from the product of the unidirectional couplings between Ca and V_m must satisfy the requirement that $(V_m \rightarrow Ca) \times (Ca \rightarrow V_m) < 0$. The latter condition also determines the relative phase of Ca and V_m alternans at the single sarcomere level, i.e., whether alternans are electromechanically concordant or discordant in the absence of spatial coupling. Under normal physiological conditions, the graded release relationship between L-type Ca current and Ca release from the SR requires that the $V_m \rightarrow Ca$ coupling is positive. Thus, in this case, the condition for instability is determined by the sign of the Ca $\rightarrow V_m$ coupling, which is itself governed by the effects of L-type Ca current and NaCa exchange current on the APD.

It is important to emphasize that the existence of the Turing-type instability elucidated here does not depend on a specific mechanism for the autocatalytic amplification of Ca alternans. Therefore, even though we have assumed here that Ca alternans are due to a steep relationship between SR release and SR load, other mechanisms of instability also could potentially give rise to a Turing instability, as long as the sign of the coupling between Ca on V_m is negative.

Our results provide a framework to interpret experimental observations of out-of-phase patterns of subcellular Ca alternans (13). In particular, they suggest that such patterns may result from a symmetry-breaking instability, rather than from intrinsic spatial heterogeneities of the Ca cycling machinery inside the cell. However, other mechanisms to form asynchronous patterns of Ca alternans are possible. Specifically, spontaneous Ca release in one region of the cell can desynchronize a spatially uniform state of in-phase Ca alternans, in an analogous way that a premature electrical stimulus can initiate out-of-phase electrical alternans in cardiac tissue (27). Therefore, to distinguish between different potential mechanisms, it is essential to experimentally determine the bidirectional coupling between Ca and V_m. The possibility of modulating this coupling is suggested by experiments in cat ventricular cells by Rubenstein and Lipsius (25), who observed a transition from concordant to discordant electromechanical alternans by reducing the temperature of the cell from 35°C to 32°C. Because theory predicts (22) that the relative phases of Ca and V_m alternans is determined by the sign of this coupling, these experiments show that this sign can be reversed by a temperature change. It therefore may be possible to validate the existence of a Turing instability experimentally by observing how the degree of synchronicity of subcellular patterns of alternans change with temperature and pacing rate.

The Turing instability elucidated here causes a spontaneous breakdown of synchrony of Ca alternans at a subcellular scale. This breakdown will generally have an influence on the dynamics of membrane voltage via Ca sensitive membrane ionic currents and hence on repolarization alternans at a single cell level. Therefore, this instability may have important implications for understanding the onset of life-threatening cardiac arrhythmias insofar as repolarization alternans at the cellular level suffice to induce wave instabilities and ventricular fibrillation at a tissue scale, as shown in both experimental and modeling studies (7, 8, 23). However, the link between subcellular and tissue scale instabilities remains to be explored. This exploration may be possible by extending the present study to networks of coupled cells.

The instability mechanism proposed by Turing (17) to explain morphogenesis based on the interaction of diffusing morphogens has been demonstrated experimentally in chemical systems that mimic reaction–diffusion models (28–30). Turing instability mechanisms also have been invoked to explain various experimentally observed patterns in biological systems (31, 32). However, the complexity of these systems makes it generally difficult to identify the morphogens that lead to the observed patterns. From this standpoint, the present work highlights the existence of a rare, and somewhat unexpected, example of a naturally occurring Turing-like instability in a biological context where the diffusing morphogens can be clearly identified. An important distinguishing feature of this instability is that one morphogen is a chemical signal (Ca), whereas the other is an electrical signal (V_m). Another distinguishing feature is that both morphogens measure the amplitudes of underlying period doubling oscillations of these signals rather than simply their magnitudes. This feature leads to a more complex interaction of the activator and the inhibitor, reflected in the reaction–diffusion model, whose manifestations in a fully nonlinear regime of this instability are yet to be explored.

1. Bers, D. M. (2002) *Nature* **415**, 198–205.
2. Bers, D. M. (2001) *Excitation-Contraction Coupling and Cardiac Contractile Force* (Kluwer, Boston).
3. Fabiato, A. (1985) *J. Gen. Physiol.* **85**, 247–289.
4. Nolasco, J. B. & Dahlen, R. W. (1968) *J. Appl. Physiol.* **25**, 191–196.
5. Chudin, E., Goldhaber, J., Garfinkel, A., Weiss, J. & Kogan, B. (1999) *Biophys. J.* **77**, 2930–2941.
6. Garfinkel, A., Kim, Y. H., Voroshilovsky, O., Qu, Z., Kil, J. R., Lee, M. H., Karagueuzian, H. S., Weiss, J. N. & Chen, P. S. (2000) *Proc. Natl. Acad. Sci. USA* **97**, 6061–6066.
7. Pastore, J. M., Girouard, S. D., Laurita, K. R., Akar, F. G. & Rosenbaum, D. S. (1999) *Circulation* **99**, 1385–1394.
8. Karma, A. (1994) *Chaos* **4**, 461–472.
9. Courtemanche, M., Glass, L. & Keener, J. P. (1993) *Phys. Rev. Lett.* **70**, 2182–2185.
10. Shiferaw, Y., Watanabe, M. A., Garfinkel, A., Weiss, J. N. & Karma, A. (2003) *Biophys. J.* **85**, 3666–3686.
11. Eisner, D. A., Choi, H. S., Diaz, M. E., O'Neill, S. C. & Trafford, A. W. (2000) *Circ. Res.* **87**, 1087–1094.
12. Diaz, M. E., O'Neill, S. C. & Eisner, D. A. (2004) *Circ. Res.* **94**, 650–656.
13. Kockskamper, J. & Blatter, L. A. (2002) *J. Physiol.* **545**, 65–79.
14. Diaz, M. E., Eisner, D. A. & O'Neill, S. C. (2002) *Circ. Res.* **91**, 585–593.
15. Fox, J. J., McHarg, J. L. & Gilmour, R. F., Jr. (2002) *Am. J. Physiol.* **282**, H516–H530.
16. Luo, C. H. & Rudy, Y. (1994) *Circ. Res.* **74**, 1071–1096.
17. Turing, A. M. (1952) *Philos. Trans. R. Soc. London Ser. B* **327**, 37–72.
18. Meinhardt, H. & Gierer, A. (2000) *BioEssays* **22**, 753–760.
19. Gierer, A. & Meinhardt, H. (1972) *Kybernetik* **12**, 30–39.
20. Franzini-Armstrong, C., Protasi, F. & Ramesh, V. (1999) *Biophys. J.* **77**, 1528–1539.
21. Wier, W. G., Egan, T. M., Lopez-Lopez, J. R. & Balke, C. W. (1994) *J. Physiol.* **474**, 463–471.
22. Shiferaw, Y., Sato, D. & Karma, A. (2005) *Phys. Rev. E. Stat. Nonlin. Soft Matter Phys.* **71**, 021903.
23. Walker, M. L. & Rosenbaum, D. S. (2003) *Cardiovasc. Res.* **57**, 599–614.
24. Euler, D. E. (1999) *Cardiovasc. Res.* **42**, 583–590.
25. Rubenstein, D. S. & Lipsius, S. L. (1995) *Circulation* **91**, 201–214.
26. Echebarria, B. & Karma, A. (2002) *Phys. Rev. Lett.* **88**, 208101.
27. Rose, K. C., Battogtokh, D., Mikhailov, A., Imbihl, R., Engel, W. & Bradshaw, A. M. (1996) *Phys. Rev. Lett.* **76**, 3582–3585.
28. Castets, V. V., Dulos, E., Boissonade, J. & De Kepper, P. (1990) *Phys. Rev. Lett.* **64**, 2953–2956.
29. Ouyang, Q. & Swinney, H. L. (1991) *Chaos* **1**, 411–420.
30. Lengyel, I. & Epstein, I. R. (1992) *Proc. Natl. Acad. Sci. USA* **89**, 3977–3979.
31. Garfinkel, A., Tintut, Y., Petrasek, D., Bostrom, K. & Demer, L. L. (2004) *Proc. Natl. Acad. Sci. USA* **101**, 9247–9250.
32. Kondo, S. & Asai, R. (2002) *Nature* **376**, 765–768.

BIOPHYSICS

PHYSICS